JOURNAL OF EXPERIMENTAL AND THEORETICAL PHYSICS, 2024, Vol. 166, No. 6 (12), pp. 815–825

ORDER, DISORDER, AND PHASE TRANSITION IN CONDENSED MEDIA

TUNNELING SPECTROSCOPY OF $BaFe_{2-x}Ni_xAs_2$ WITH VARIATION OF DOPING DEGREE IN SUPERCONDUCTING AND NORMAL STATES

© 2024 I. A. Nikitchenkov[a,b], S. A. Kuzmichev[a,b]*, A. D. Ilina[b], K. S. Pervakov[b], V. A. Vlasenko[b], T. E. Kuzmicheva[b]

[a] Lomonosov Moscow State University, Faculty of Physics, Moscow, 119991 Russia

[b] Lebedev Physical Institute of the Russian Academy of Sciences, Moscow, 119991 Russia

* e-mail: kuzmichev@mig.phys.msu.ru

Received June 05, 2024

Revised August 02, 2024

Accepted August 03, 2024

Abstract. Single crystals of pnictides $BaFe_{2-x}NixAs_2$ with underdoped composition ($x = 0.08$) and overdoped compositions ($x = 0.12, 0.14$) were studied by tunneling spectroscopy in superconducting and normal states. The obtained *I(V)*- and *dI(V)/dV* characteristics of tunnel contacts reproducibly showed nonlinearity both below and above the critical temperature T_c, not directly related to superconducting properties. Its evolution with temperature and T_c along the doping phase diagram was studied, and possible causes of this nonlinearity existence are discussed.

The article is presented as part of the proceedings of the 39th Low Temperature Physics Meeting (LT-2024), Chernogolovka, June 2023.

DOI: 10.31857/S004445102412e071

1. INTRODUCTION

Among the variety of iron-based high-temperature superconductors (HTSC), [1, 2] ferropnictides of the 122 structural family have been most thoroughly studied both theoretically and experimentally. Researchers' interest in this type of compounds was primarily due to the significant critical magnetic fields at moderate critical temperatures T_c of the 122 family, as well as the availability of large qualitative single crystals are the factors that determined the development of technical applications of Ba-122 for the production of superconducting (SC) magnets and wires [3, 4].

The crystal structure of Ba-122 family compounds contains superconductivity-responsible blocks Fe–As, alternating with mirror symmetry and separated along the *c*-direction by barium planes. In the stoichiometric composition $BaFe_2As_2$ demonstrates ordering into an antiferromagnetic (AFM) state with a spin density wave. Slightly above the Néel temperature at $T_N \approx T_s \approx 138$ K a structural phase transition occurs from orthorhombic to tetragonal symmetry. With partial substitution of iron with nickel, the AFM phase is gradually suppressed, and a SC-region emerges in the form of a doping "bell" with maximum $T_c \approx 21$ K, achieved at the optimal substitution degree in the composition $BaFe_{1.9}Ni_{0.1}As_2$ [5].

The electronic properties of the 122 system are determined by iron 3*d*-orbitals and possess a clearly pronounced quasi-2D character. These compounds are characterized by conductivity anisotropy between the *ab*- and *c*-directions of the crystal [5]. The Fermi surface contains hole barrels slighltly corrugated along the momentum k_z-direction near the Γ-point of the Brillouin zone, as well as electron pockets near the X-point, forming propellers or barrels depending on the chemical composition [6–8]. For $BaFe_{2-x}Ni_xAs_2$ band structure studies using angle-resolved photoemission spectroscopy (ARPES) have not been conducted; however, for the parent compound and $BaFe_{2-x}Co_xAs_2$ of the 122 family, a proximity to the Lifshitz transition was shown, along with the presence of a "flat band" and

peaks in the density of electronic states $N(E)$ near the Fermi level [7, 8]. Some ARPES studies for the Ba-122 system [9] also reported anomalous band structure shifting with temperature increase up to room temperature.

When studying compounds $Ba(Fe,Ni)_2As_2$ below T_c researchers mainly observe two SC-condensates with different order parameters, Δ_L and Δ_S, called the large and the small SC gaps respectively. Our group previously determined the BCS theory characteristic ratios for these gaps in single crystals $Ba(Fe,Ni)_2As_2$ with different doping levels: $2\Delta_L(0)/k_BT_c \approx 4$–$6$ for the large SC gap (the range of values is caused by its presumed anisotropy in the k-space) and $2\Delta_S(0)/k_BT_c \approx 2$ for the small SC gap, both practically independent of nickel substitution degree in a wide range of T_c [10–12]. Similar values were obtained using THz and infrared Fourier spectroscopy [13, 14]. However, not all experimental methods agree well when studying the gap structure $BaFe_2As_2$. The quasi-2D structure of the compound makes the system extremely sensitive to measurement conditions. This can lead to discrepancies in data obtained using surface, bulk, and local methods; in particular, ARPES studies conducted by different groups poorly agree when determining the characteristic ratio of the large SC gap, with a spread of $2\Delta_L(0)/k_BT_c \approx 4.5-7.5$ for $BaFe_2As_2$ with various doping levels (for review see [7, 15]).

The question of the leading pairing mechanism in ferropnictides remains a relevant topic. In addition to spin fluctuations caused by nesting of momentum-space separated Fermi surface sheets [16], researchers propose orbital fluctuations of $3d$ orbitals of Fe [17] for this role. However, orbital degrees of freedom gain additional significance when discussing properties in the normal state, such as the nematic phase, defined as spontaneous breaking of rotational symmetry C_4 without breaking translational symmetry. Such symmetry breaking manifests in the anisotropy of electronic properties; particularly, when studying the compound $Ba(Fe,Co)_2As_2$ using ARPES, signs of nematic order were discovered in the form of energy splitting of d_{xz}/d_{yz}-orbitals, occurring at temperatures even higher than T_s and T_N [18, 19, 20]. Another discussed feature of the normal state of ferropnictides is the pseudogap [20–22], previously observed in HTS cuprates [23, 24]. As one of the main mechanisms for pseudogap formation in cuprates, researchers highlight the residual dielectrization of the spectrum associated with spin/charge ordering in the system [25]. However, while the parent compound of cuprates is an AFM insulator, the parent compound of pnictides $BaFe_2As_2$ has a metallic ground AFM state [5]. The pseudogap remains a mysterious state of the electronic subsystem, with no consensus reached about its nature [23-25]. Overall, despite intensive research into the physics of iron-containing pnictides, the question of the relationship between superconductivity and normal state features such as magnetic order, nematic phase, band structure, and pseudogap [8, 16, 17, 22, 26, 27] remains debatable.

In this work, we present a thorough study of $BaFe_{2-x}Ni_xAs_2$ ferropnictide properties using tunneling spectroscopy methods. The three compositions were studied: with nickel content $x = 0.08$, belonging to the underdoped region of the phase diagram, and two overdoped compositions with $x = 0.12$, 0.14. Previously, during the study of the gap structure for tunnel contacts in $BaFe_{1.86}Ni_{0.14}As_2$ and $BaFe_{1.9}Ni_{0.1}As_2$ our group discovered reproducible features in the dynamic conductance spectra $dI(V)/dV$, uncharacteristic for the classical case and manifesting in both SC and normal states [11]. The temperature behavior of these features was studied in more detail for the system $BaFe_{1.88}Ni_{0.12}As_2$ [28], however, their origin remains ultimately unknown. This work reveals the behavior of these normal state features with varying doping levels, covering under- and overdoped regions of the phase diagram. Based on the obtained experimental data, an analysis of possible causes for the studied normal state nonlinearity is conducted, and the nature of the observed effect is discussed.

2. EXPERIMENTAL TECHNIQUE

The $BaFe_{2-x}Ni_xAs_2$ single crystals studied here with nominal doping nickel concentration $x = 0.08$, 0.12, 0.14 were grown using the "self-flux" technique [15, 29–31]. The synthesized single crystals were characterized by X-ray diffraction, confirming the sample's correspondence to the 122-phase. Energy-dispersive spectroscopy revealed the ratio of elements present in the single crystal, consistent with the batch composition. As a result of measuring the temperature dependencies of resistance and

magnetic susceptibility, a phase transition to the SC state was detected in the samples, and the critical transition temperature $T_c \approx 18, 19, 12$ K was determined for single crystals with nickel content $x = 0.08$, 0.12, 0.14 respectively [10–12, 15, 29–31].

To obtain tunnel contacts of superconductor-constriction-superconductor (ScS) type, the planar "break-junction" technique was used, which involves creating a contact by mechanical splitting of a layered sample at low temperatures [32, 33]. In preparation, the studied single crystal sample, having the shape of an elongated plate with dimensions of about $3 \times 1 \times 0.1$ mm^3, is fixed using In-Ga-solder drops (liquid at room temperature) in a fourcontact connection scheme on massive copper electrodes located on a U-shaped spring holder equipped with a stress concentrator. The degree of the holder bending during the experiment is regulated mechanically and precisely. The layered sample is mounted so that the *ab*-plane of the crystal is parallel to the holder plane. After mounting, the holder with the sample is cooled to 4.2 K. At this point, the solidified In–Ga-solder rigidly fixes the sample. When the table is bent under the single crystal delaminates along the *ab*-planes of the crystal lattice, forming a tunnel contact on natural steps and terraces separating two cryogenic cleavages along the *c*-direction. As a result, the tunnel current always flows in the *c*-direction of the crystal. The moment of cryogenic cleavage formation is objectively monitored by the appearance of a finite I–V characteristic slope in real time. The massive SC banks of the obtained ScS contact provide effective heat removal from the contact interface. Note that mechanical contact adjustment remains available throughout the measurement process, opening the possibility for direct local probe of bulk energy parameters in various cleavage regions, i.e., collecting statistics with one and the same sample during a single experiment.

Strictly speaking, the obtained break junctions represent a structure of S–n–I–n–S type (I — insulator, where n–I–n acts as a barrier), in which the barrier transparency is described by the dimensionless parameter Z [34, 35]. In single crystals of the $BaFe_2As_2$ family, the cleavage usually occurs along the barium metallic planes [36]. It should also be noted that since during the experiment the microcrack remains deep in the bulk of the sample (the contact banks are not separated), this naturally protects the cryogenic cleavage site from degradation and impurity contamination. Thus, in the used "break-junction" configuration, it is most likely to obtain highly transparent ScS contacts with transparency above 80% ($Z < 0.5$), which is confirmed by the features of of I–V characteristics and $dI(V)/dV$-spectra (see below).

Although the planar "break-junction" technique can provide single contacts, often the tunnel structures obtained in the experiment represent a natural array of m (where m is a natural number) equivalent ScS contacts forming a stack due to objective geometric features of layered compounds. The configuration and characteristic features of our planar mechanically adjustable break-junction experiment are discussed in more detail in review [33].

In an SnS contact with a quasiparticle transport close to ballistic (contact diameter d much smaller than the mean free path of quasiparticles $d \ll l$), at temperatures below T_c the effect of multiple Andreev reflections is realized [34, 35, 37]. In general, in the "long" SnS contact mode (with incoherent $d \gg \xi$ transport), the incoherent multiple Andreev reflections effect (IMARE) is observed. The effect causes excess current in the I–V characteristic of the SnS contact at any bias voltages (relative to I–V characteristic at $T > T_{\tilde{n}}$). At bias voltages $eV \to 0$ in the $dI(V)/dV$ spectrum, a so-called "foot" region of increased conductivity appears (compared to the normal state I–V curve), and the gap features (minima) at $|eV_{i,n}| = 2\Delta_i/n$. The number of n observed minima decreases at small ratios l/d [37, 38], as well as with increasing barrier strength Z [34, 35] and the broadening parameter Γ. The local T_c of the contact (corresponding to the transition of the contact area of size 10–50 nm to the normal state) was determined as the temperature at which all features caused by IMARE transport disappeared in the $dI(V)/dV$ spectrum.

In $dI(V)/dV$ spectrum of a stack of m contacts, the position of all features caused by bulk properties increases by m times, in particular, for Andreev structures $|eV_{i,n}| = m \cdot 2\Delta_i/n$. For single crystals of each composition, the number m is determined by comparing the obtained $dI(V)/dV$-spectra of stacks with different m (normalization details are provided in the

appendix to works [11,39]). The advantage of stack contacts lies in the prevalence of bulk material properties, which allows minimizing the influence of surface defects [33]. For the I–V characteristics and $dI(V)/dV$ spectra shown below, the bias axis is normalized to the corresponding m ($V_{norm} \equiv V/m$).

3. RESULTS

Figure 1 shows I–V characteristics and differential conductance spectra of tunnel contacts obtained for single crystals $BaFe_{2-x}Ni_xAs_2$ with different doping levels and T_c. The bias axis is normalized to the number of contacts in the stack $m = 14, 7, 20$ in the Figures 1*a*, *b*, *c* respectively. In the SC state at a temperature of 4.2 K at small eV, the spectra show characteristic Andreev features, and there is no supercurrent branch on the I–V curve. Thus, based on the I–V characteristics and $dI(V)/dV$-spectra, it can be established that the contacts in Fig. 1 are "long" and are in an incoherent SnS mode in accordance with the predictions [34, 35, 37]. Fig. 1*a* shows the $dI(V)/dV$-spectrum of an SnS contact obtained in a slightly underdoped single crystal $BaFe_{1.92}Ni_{0.08}As_2$ at $T = 4.2$ K (red curve) and above T_c at $T = 19$ K (dark yellow curve). In the SC state, the spectrum contains gap minima ($n_i = 1$), corresponding to three SC order parameters: $\Delta_L^{out} \approx 4.4$ meV, $\Delta_L^{in} \approx 3$ meV (presumably belonging to the same SC condensate, anisotropic in k-space) and $\Delta_S \approx 1.1$ meV at $T \ll T_c$, previously determined for this compound [10] (intragap region marked in gray), as well as an Andreev conductance peak at zero bias (pedestal). Besides Andreev features, $dI(V)/dV$ spectrum contains a general nonlinearity – maximum-minimum structure at biases of$eV_{max} \approx 20$ meV and $eV_{min} \approx 50$ meV – in a wide range of voltages. These bias voltages significantly exceed the amplitudes of SC-order parameters of about $2\Delta_i(0)$. It is clearly seen that at $T = 19 > T_c$ the Andreev features disappear, while the nonlinearity shape and positions of eV_{max} and eV_{min} remain unchanged: red and dark yellow curves in Fig. 1*a* at eV > $2\Delta_L^{out}$ almost coincide. Note that the invariance of dynamic conductance of this contact with temperature at $eV > 2\Delta(0)$ indicates the ballistic nature of transport in accordance with [40, 41].

Similar nonlinearity, related to normal state features, is also observed in single crystals of $BaFe_{2-x}Ni_xAs_2$ with different nickel doping content

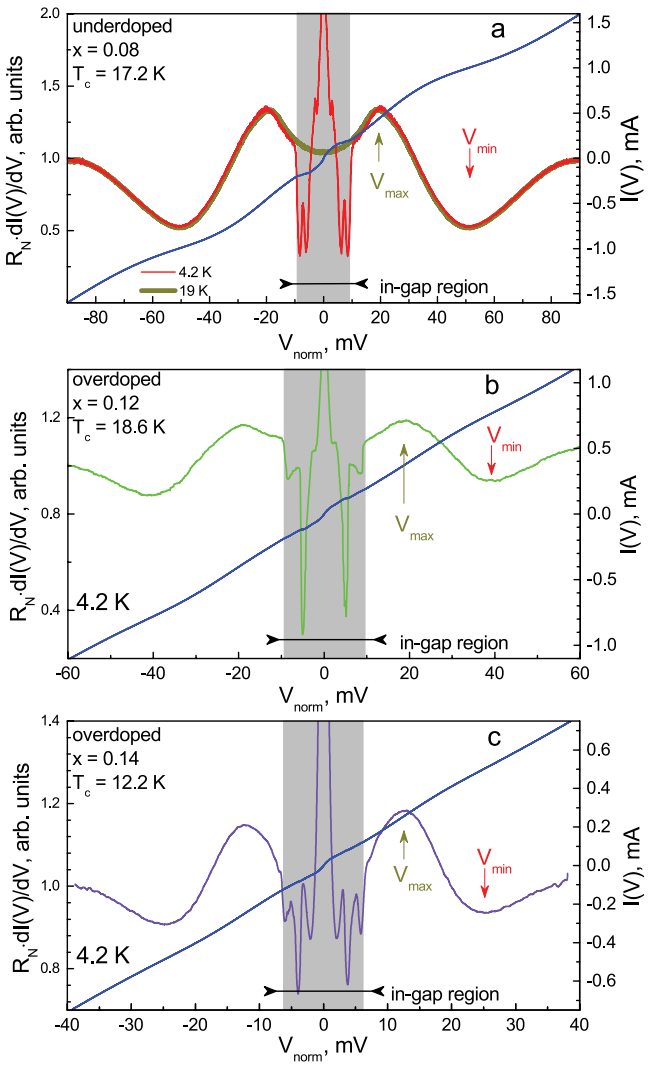

Fig. 1. I–V curve (blue line, right axis) and its corresponding $dI(V)/dV$-spectrum (left axis), measured at $T = 4.2$ K for the SnS contact in compound $BaFe_{2-x}Ni_xAs_2$, where: *a* — $x = 0.08$ ($m = 14$ contacts in the stack), *b* — $x = 0.12$ ($m = 7$), *c* — $x = 0.14$ ($m = 20$). For comparison, Fig. 1*a* shows the $dI(V)/dV$-spectrum measured at temperature $T = 19\,\text{K} > T_c$ (dark yellow curve, left axis). Gray color marks the in-gap bias regions containing Andreev features of the SC order parameters. Vertical arrows mark the positions of $dI(V)/dV$ features persisting in the normal state – maxima V_{max} and minima V_{min}. All dynamic conductance spectra are normalized to normal conductance at large bias $G_N \equiv 1/R_N(eV \gg \Delta(0))$

(Figs. 1*b*, *c*). In overdoped compositions with increasing $x = 0.12 - 0.14$ SC-order parameter amplitudes decrease almost proportionally to T_c [10, 11, 12], and the positions V_{min} and V_{max} also shift towards lower biases: $V_{max} \approx 20$ mV, $V_{min} \approx 40$ mV for composition with $x = 0.12$, $V_{max} \approx 12$ mV; $V_{min} \approx 25$ mV for $x = 0.14$.

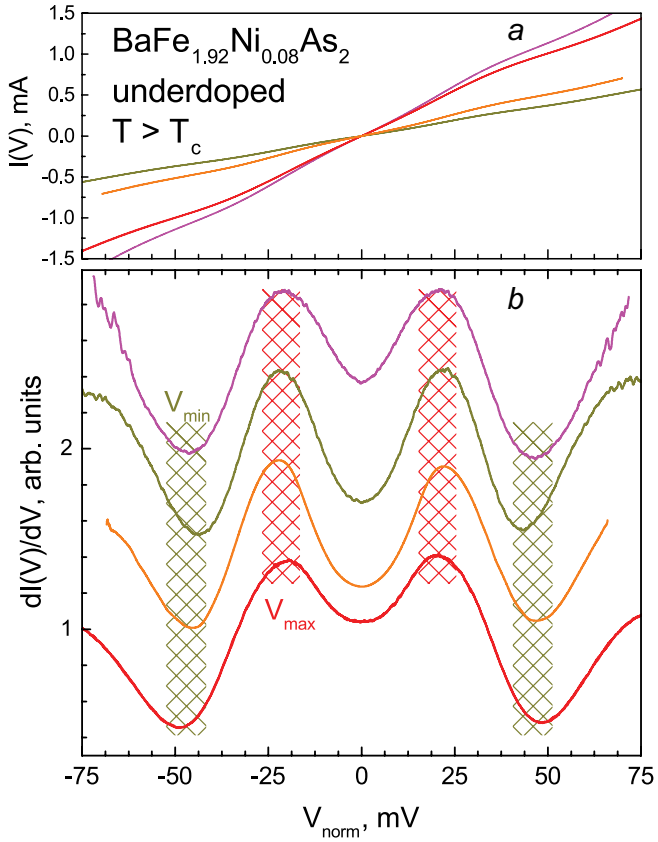

Fig. 2. Measured at $T > T_c$ I-V curves (*a*) and corresponding dynamic conductance spectra (*b*) of SnS contacts obtained in different underdoped single crystals of composition $BaFe_{1.92}Ni_{0.08}As_2$ from the same batch. Hatched areas mark regions where maxima V_{max} and minima V_{min} of the nonlinearity caused by normal state features are reproducibly observed. $dI(V)/dV$ spectra are normalized to $G_N \equiv 1/R_N$ and shifted vertically for convenience

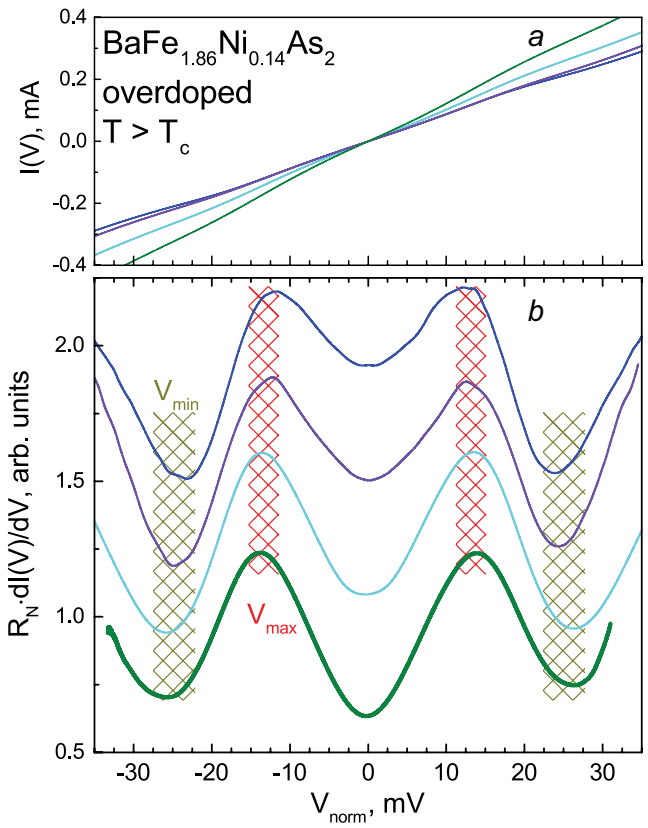

Fig. 3. Measured at $T > T_c$ I–V characteristics (*a*) and corresponding dynamic conductance spectra (*b*) of SnS-contacts obtained in different single crystals of overdoped composition $BaFe_{1.86}Ni_{0.14}As_2$ from the same batch. Hatched areas mark regions where maxima V_{max} and minima V_{min} of nonlinearity caused by the normal state features are reproducibly observed. $dI(V)/dV$ spectra are normalized to $G_N \equiv 1/R_N$ and shifted vertically for convenience

To verify the reproducibility of the observed nonlinearity in the normal state, significant statistics of $I(V)$ and $dI(V)/dV$-characteristics of tunnel junctions were collected. Examples of I–V curves and corresponding differential conductance spectra at $T > T_c$ for stacks with different numbers of contacts m, obtained in single crystals $BaFe_{1.92}Ni_{0.08}As_2$ and $BaFe_{1.86}Ni_{0.14}As_2$, are shown in Figs. 2 and 3 respectively; similar data for $BaFe_{1.88}Ni_{0.12}As_2$ are shown in Fig. 2*c* in [28]. For each composition, the I–V curves have different slopes, consequently, the normal resistance R_N of the presented contacts, which, in turn, is determined by geometric parameters and contact area. Nevertheless, the general shape of the spectrum nonlinearity and the bias voltages V_{min} and V_{max} are reproduced. Thus, the observed nonlinearity is related to the intrinsic, bulk properties of the normal state $BaFe_{2-x}Ni_xAs_2$ and cannot be caused by random effects or geometric resonances.

Temperature evolution of nonlinear $dI(V)/dV$ spectra and positions of features V_{min} and V_{max} were studied for tunnel junctions based on $BaFe_{1.92}Ni_{0.08}As_2$ and $BaFe_{1.86}Ni_{0.14}As_2$ and are presented in Figs. 4, 5. For the shown contacts $R_N(T) \approx$ const. In Figs. 5*b* and 6*b* for convenience, the spectra were manually shifted by a constant value along the ordinate axis. Characteristic Andreev features of the spectra associated with the IMARE disappear when the local critical temperature of the contact is reached. The shape of nonlinearity associated with the normal state features remains preserved with increasing temperature, the positions of features $dI(V)/dV$ within the margin of error remain unchanged throughout the entire studied temperature range $T = 4.3$–38.2 K. Similar

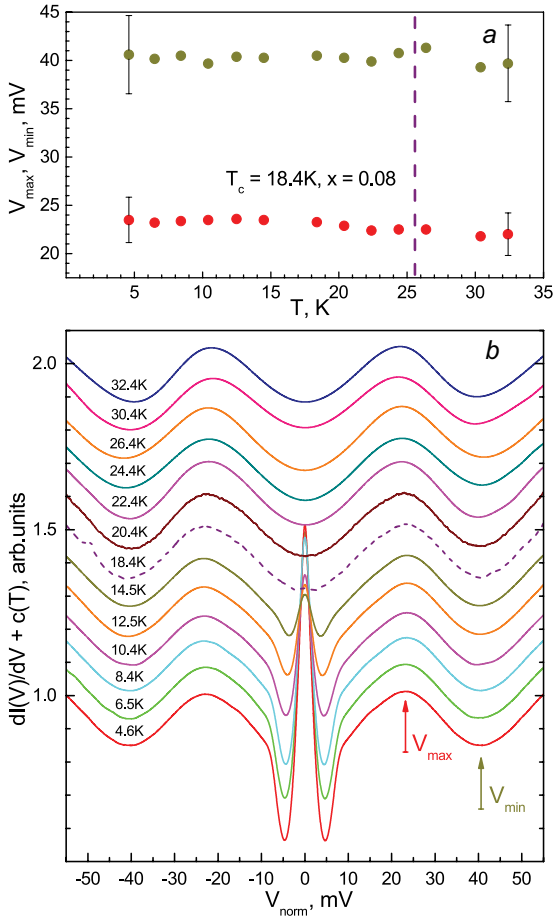

Fig. 4. Temperature evolution of the positions of maximum V_{max} and minimum V_{min} of nonlinearity caused by the normal state features (*a*) and corresponding $dI(V)/dV$ spectrum of tunnel junction in single crystal $BaFe_{1.92}Ni_{0.08}As_2$ (*b*). The dashed line corresponds to the local critical temperature of the contact $T_c \approx 18.4$ K. The curves are manually shifted vertically by a constant value for convenience, $R_N(T) \approx$ const

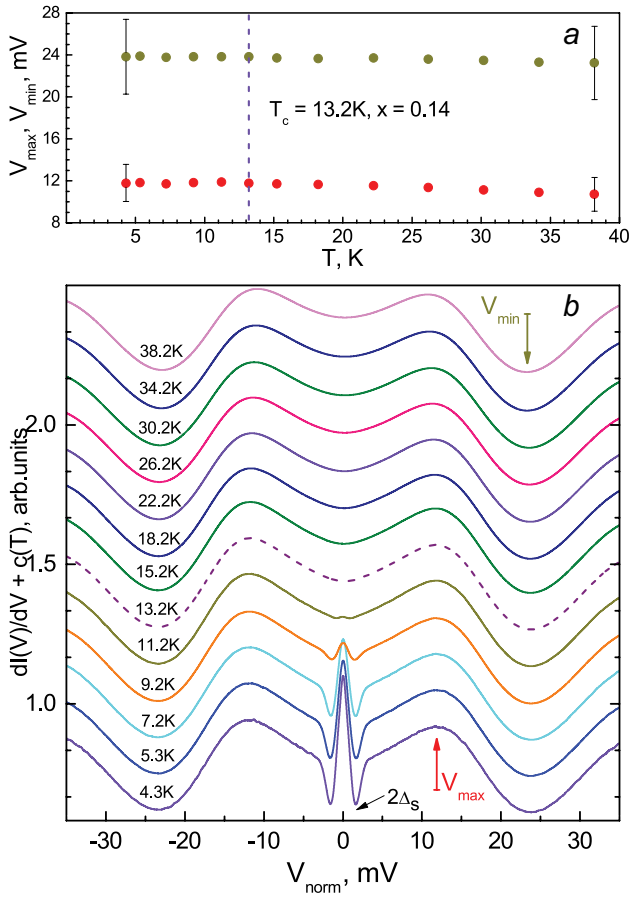

Fig. 5. Temperature evolution of the positions of maximum V_{max} and minimum V_{min} of the nonlinearity caused by the normal state features (*a*) and corresponding $dI(V)/dV$ spectrum of tunnel contact in single crystal $BaFe_{1.86}Ni_{0.14}As_2$ (*b*). The dashed line corresponds to the local critical temperature of the contact $T_c \approx 13.2$ K. The curves are manually shifted vertically by a constant value for convenience, $R_N(T) \approx$ const. Arrows mark the positions of Andreev features of the small SC-gap $2\Delta_S$ at 4.3 K

temperature-independent behavior of the normal state features in single crystals $BaFe_{1.88}Ni_{0.12}As_2$ was observed in Fig. 4 in [28].

4. DISCUSSION

Fig. 6 shows a doping evolution of the positions of maximum V_{max} and minimum V_{min} of the nonlinearity on $dI(V)/dV$ spectra of contacts with different local T_c, obtained in under- and overdoped samples $BaFe_{2-x}Ni_xAs_2$ (the correspondence between T_c and substitution degree x is provided according to the data from work [31]). As the concentration of doping nickel increases, the values of the observed features' positions decrease almost linearly, on average covering the range from $V_{max} \approx 22$ mV, $V_{min} \approx 49$ mV at $x = 0.08$ to $V_{min} \approx 13$ mV, $V_{max} \approx 26$ mV at $x = 0.14$. Thus, unlike the SC-order parameters [5,10–12], the values V_{min} and V_{max} respond to chemical doping monotonically and do not describe a "bell" near the optimal doping region of the phase diagram. This further indicates that the discovered spectral feature is not directly related to the SC-order parameter. Features at V_{min} and V_{max} converge with increasing nickel content as they move away from the parent compound $BaFe_2As_2$ and the phase diagram region containing magnetic and structural phase transitions. Linear approximation predicts that the position of features will reach the Fermi level ($V_{min}, V_{max} \to 0$) at the doping level $x \to 0.22$, which corresponds to a heavily overdoped, non-superconducting composition.

We emphasize again that the reproducible nonlinearity of dynamic conductance observed in the spectra of stack contacts unambiguously indicates the bulk nature of this effect. Let us discuss possible causes of nonlinearity $dI(V)/dV$ in the normal state.

1) It is known that in a tunnel contact being in the thermal regime ($l \ll d$), quasiparticle transport is dissipative: when a measuring current is applied, the temperature inside the contact T_{pc} increases relative to the ambient temperature T_{bath} with increasing bias eV as [42]

$$(k_B T_{pc})^2 = (k_B T_{bath})^2 + (eV)^2/4L, \qquad (1)$$

where L is the Lorenz number. In Fig. 7, dashed lines show model $dI(V)/dV$-spectra for thermal contacts undergoing an overheating (whose resistance has a temperature dependence corresponding to that of $R(T)$ bulk single crystal). The curves were calculated for $BaFe_{2-x}Ni_xAs_2$ with $x = 0.08$ (*a*) and $x = 0.14$ (*b*) based on formula (1) and the dependence $T(R)$, obtained from experimental resistive curve data of corresponding bulk single crystals (in the insets). The different shape of model curves for contacts based on under- and overdoped samples is due to the features of $R(T)$: the presence of structural and magnetic transitions in the crystal with $x = 0.08$ at $T_s \approx 65$ K, where a minimum of $R(T)$, is observed, and their absence in the crystal with $x = 0.14$, showing monotonic resistance growth above T_c. It is evident that for $x = 0.14$ (Fig. 7*b*) the model curve does not correspond to the dynamic conductance of NcN-contact (N bulk normal metal) observed in the experiment above T_c (solid line), therefore, the nonlinearity of $dI(V)/dV$ cannot be caused by contact overheating. Although for the underdoped composition, the calculated spectrum of the thermal contact is similar to the experimental one (Fig. 7*a*), we note that our obtained tunnel contacts are in the ballistic regime ($l > d$), which is controlled by the invariance of normal conductance at zero bias G_{ZBC} with temperature above T_c, in accordance with the invariance pl for a Sharvin contact (where p is the material resistivity). As an example, the left inset to Fig. 7*a* shows the dependence $G_{ZBC}(T)$ for the tunnel contact based on $BaFe_{1.92}Ni_{0.08}As_2$ (stars) compared to the bulk single crystal conductance $G_{bulk}(T)$ of this composition (line). It is clearly seen that in the studied temperature range from 18.4 to 54 K, the change in $G_{bulk}(T)$ is about 11%, while $G_{ZBC}(T)$ remains approximately constant (value scatter does not exceed ±2%). Thus, in the obtained tunnel contacts, there is no heat generation during measurement current flow, and the observed nonlinearity $dI(V)/dV$ also cannot be caused by overheating.

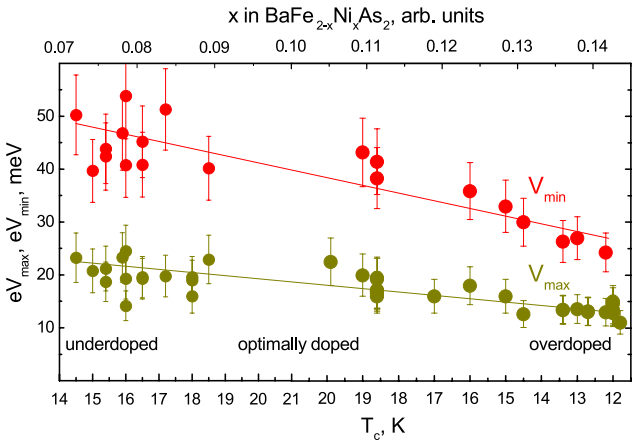

Fig. 6. Dependence of maximum positions V_{max} and minimum V_{min} of the nonlinearity caused by the normal state features on T_c and its corresponding doping level x, (the relative x is taking from [31])

2) One possible explanation for the nonlinearity we observe in the dynamic conductance spectrum may lie in an unusual interaction between the measurement current and the resulting stacked tunnel structure. Let's assume, for example, that the latter consists of twins, with an even number of contacts giving an equal number of domains oriented in both directions, and their twin boundary sequence along the current flow line is electrically equivalent to an equal number of p–n- and n–p-interfaces, connected in series. The scheme of such assembly for two pairs of elements is shown in Fig. 7*c* below. Usually, the symmetry of I–V characteristic and its $dI(V)/dV$-spectrum proves the absence of Schottky-type barriers. However, due to the symmetry of the specified assembly, its I–V characteristic will also be symmetric but will have features related not to the intrinsic properties of the material but to the sample structure, which has no fundamental significance.

Let's consider an exceptional case where the I–V symmetry cannot indicate the absence of Schottky barriers. In general, spectra resembling experimental ones in shape can be obtained by considering the experimental tunnel structure as an electrical circuit

consisting of a central resistor R_0 (reflecting the normal "Sharvin" conductance of the contact), and a set of $2i$ counter-series Schottky diodes with ideal current-voltage characteristics $I_i(V) = d_i(e^{\beta_i V} - 1)$, shunted by equivalent resistances r.

We calculated the I–V characteristics and corresponding $dI(V)/dV$-spectra for the above assembly of two pairs of diodes (yellow curve in Fig. 7*c*, $i = 1, 2$) and a similar assembly of four pairs of diodes (blue curve, $i = 1 - 4$). The case of three diodes is not considered since it gives a decrease in tunnel contact conductance at increased bias voltage, which does not correspond to the experiment. In order to fit the dip-hump features in the $dI(V)/dV$, we used d_i and β_i as free parameters. As a result, although the general shape of the calculated curves corresponds to the behavior of dI/dV in the studied bias range, the amplitude of the calculated nonlinearity $(G(V_{max}) - G(V_{min}))/G(V_{max})$ even with optimal parameters (implementing maximum amplitude) of the diode assembly, does not exceed 2–3%, while the experimental dependence gives values at approximately 40% (note that the calculated curves refer to the right axis of Fig. 7*c*, whose scale is increased 5 times relative to the left axis for clarity). Generally speaking, by varying the values of d_i and β_i one can achieve significant amplitude features, but then their positions would differ several times from those observed experimentally. Thus, it is impossible to satisfactorily fit the calculated spectra to the experimental ones, as their amplitudes differ by approximately an order of magnitude, and we exclude this possibility from consideration.

3) According to the well-known phenomenological approach by Giaever and Megerle [43], the I–V characteristic of a symmetric NcN-contact with low transparency depends on the distribution of metal electron density of states (EDOS) near the Fermi level E_F and is described by the following expression:

$$I(V) = A' \int_{-\infty}^{\infty} N(E)N(E + eV)(f(E) - f(E + eV)dE, \quad (2)$$

where À′ is a geometric factor, $N(E)$ is the metallic distribution function of EDOS, $f(E)$ is the equilibrium Fermi-Dirac distribution.

In the quasi-classical case in the vicinity of E_F the distribution $N(E) \approx N_0 = \text{const}$, and the resulting I–V characteristic has a conventional linear (ohmic) form. If the distribution $N(E)$ contains nonlinearities caused, for example, by features of the compound's band structure or renormalization of the density of states due to interaction with characteristic bosonic modes in the system, the I–V characteristic may deviate from the linear law, providing experimental information about the behavior of function $N(E)$ near the Fermi level. For example, the, $dI(V)/dV$-spectrum obtained using a scanning tunneling microscope (STM), when the STM tip does not contact the sample surface, corresponds to the case of $N'cN$ contact with low transparency and is proportional to the distribution $N(E)$ in the studied material "N" assuming monotonic $N^*(E)$ for the metal N'-STM tip.

Unfortunately, at present, the authors are unaware of theoretical calculations for Ba-122 with iron substitution by Ni with sufficient detail of the density of electronic states $N(E)$ near the Fermi level that would allow calculation of I–V characteristics within the Giaever and Megerle approach. We are also unaware of experimental works studying $BaFe_{2-x}Ni_xAs_2$ using STM spectroscopy that would obtain $dI(V)/dV$-spectra above T_c in a wide range of biases.

As a rough estimate, we took $dI(V)/dV$ spectrum obtained using STM for the related $BaFe_{1.79}Co_{0.21}As_2$ overdoped composition with electron substitution and $T_c \approx 13$ K (upper curve above T_c in Fig. 3*a* in [44]) as $N(E)$ and calculated the corresponding $dI(V)/dV$ spectrum of tunnel junction using formula (2). The calculation result is shown in Fig. 8 by dashed orange line. It can be seen that although the calculated curve contains a wave-like structure, it cannot describe the experimentally observed nonlinearity in $BaFe_{1.86}Ni_{0.14}As_2$ with similar T_c. Nevertheless, considering that the Fermi level position in energy is affected not only by the substitution degree (number of doping electrons per Fe atom) but also by the unit cell size (chemical pressure) related to dopant atom radius, one can try to reproduce the experimental spectrum by slightly shifting the Fermi level (zero bias) in the initial $N(E)$ curve, taken from [36]; the corresponding family of calculated spectra is shown in Fig. 8 by thin lines, with a shift step $\Delta E = 7$ meV. Indeed, by raising E_F by only 17 meV (solid dark green curve in Fig. 8), it is possible not only to obtain a typical dip-hump shape (although of smaller amplitude) but also to accurately reproduce their positions

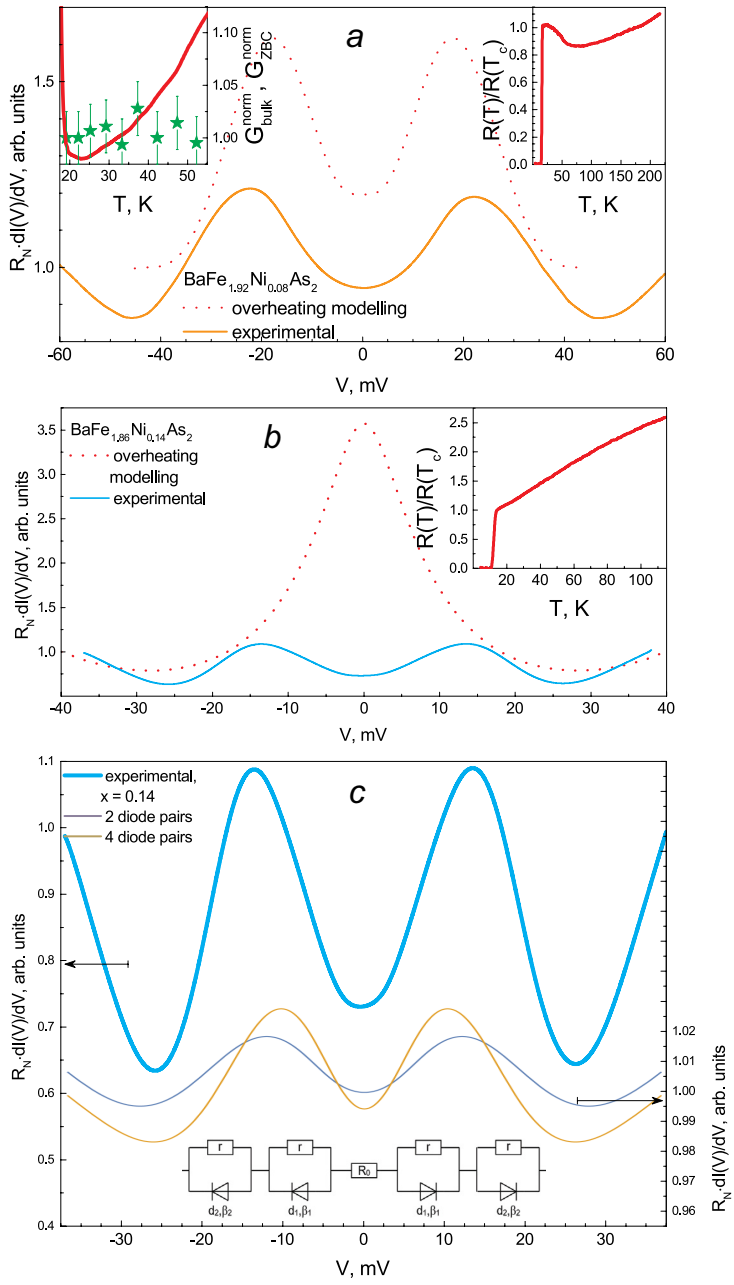

Fig. 7. *a* — Comparison of experimental $dI(V)/dV$ spectrum of tunnel contact at $T > T_c$ (solid line) with the model spectrum for NcN-contact in thermal regime undergoing an overheating overheating (dashed line), calculated based on formula (1) and dependence $R_{bulk}(T)$ of bulk sample of underdoped composition with $x = 0.08$ (right inset). The left inset shows the dependence of bulk conductance $G_{bulk} \equiv 1 / R_{bulk}$ (line) and zero-bias conductance of tunnel contact (stars). $G_{norm} \equiv G(T)/G(T_c)$. *b* — Similar data for heavily overdoped sample with $x = 0.14$. *c* — Comparison of experimental $dI(V)/dV$-spectrum of tunnel contact at $T > T_c$ (left axis, solid line, similar to that shown in Fig. *b*) with dynamic conductance of assemblies (right axis), containing two pairs of diodes (shown below; yellow curve) and four similar pairs of diodes (blue curve)

$eV_{max} \approx 14$ meV, $eV_{min} \approx 24$ meV (solid purple line in Fig. 8), observed experimentally for composition $BaFe_{1.86}Ni_{0.14}As_2$.

It is interesting to note that observed by ARPES [18–20] both in nematic phase and outside it (see Fig. 5*b* [20]) asymmetry of bands formed by d_{xz} and d_{yz} Fe orbitals can cause nonlinearity of $N(E)$: inequivalent energy positions of these bands correspond to two maxima of $N(E)$. According to [18, 20], band structure symmetrization occurs at a significant distance from the nematic phase.

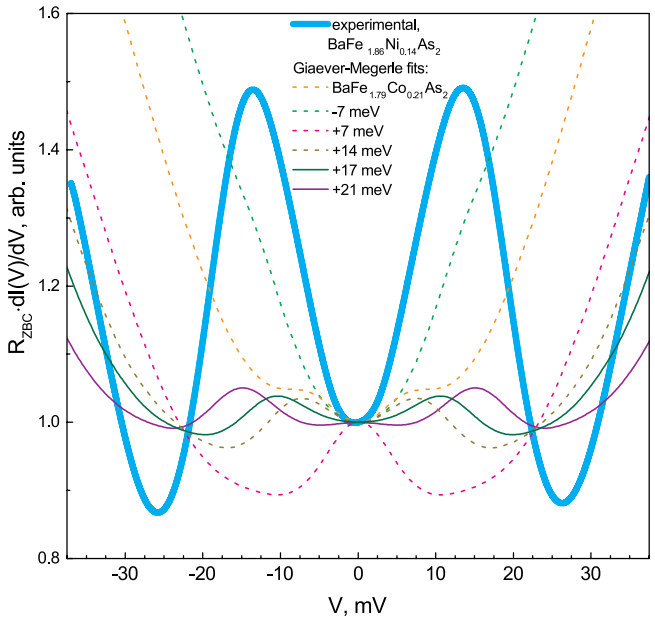

Fig. 8. Comparison of experimental $dI(V)/dV$ spectrum of tunnel junction at $T > T_c$ (bold line, similar to the one shown in Fig. 7*b*, *c*) with model $dI(V)/dV$-spectra calculated using formula (2) based on STM data for $BaFe_{1.79}Co_{0.21}As_2$ [44] (orange dashed line) and with Fermi level shift relative to data [44]

One can expect the appearance of maximum-minimum structures on $N(E)$ (consequently, in the $dI(V)/dV$ spectrum of tunnel contact in the normal state) in both under- and overdoped compositions, similar to those obtained in our experiment. The observed "convergence" of V_{max} and V_{min} with increasing substitution degree (i.e., when moving away from the nematic phase) and their extrapolated disappearance in the nonsuperconducting composition ($x \approx 0.22$) also qualitatively agrees with Fig. 5 in [20] and, accordingly, with this assumption about the nature of nonlinearity in $dI(V)/dV$ spectra in the normal state.

To verify the above assumption about the nature of the nonlinearity we observed in $dI(V)/dV$ spectra of tunnel contacts above T_c additional studies of $N(E)$ near E_F in $BaFe_{2-x}Ni_xAs_2$ and its evolution along the doping phase diagram are required using ARPES methods, as well as tunnel and optical spectroscopy.

5. CONCLUSIONS

In $I(V)$ and $dI(V)/dV$-characteristics of tunnel contacts created in single crystals of $BaFe_{2-x}Ni_xAs_2$ pnictides of under- and overdoped composition ($x = 0.08$, 0.12, 0.14 with $T_c \approx 12 - 19$ K), a strong residual nonlinearity was reproducibly observed both below and above T_c, not directly related to the superconducting properties. It is shown that the nonlinear form of $dI(V)/dV$-spectra, representing a maximum-minimum at bias voltages $eV_{max}, eV_{min} > 2\Delta(0)$, cannot be caused by geometric resonances or the macrostructure of a particular single crystal (for example, twin formation), but has, on the contrary, a bulk nature due to the intrinsic properties of the material. In overdoped compositions (when moving away from AFM and nematic phases), the bias voltages eV_{max}, eV_{min} decrease, while linear extrapolation towards increasing substitution degree x predicts the disappearance of these features and linearization of the $dI(V)/dV$ spectrum of the tunnel contact in nonsuperconducting composition at $x \approx 0.22$. The most probable cause of the nonlinearity in I–V characteristics and $dI(V)/dV$ spectra is presumed to be the presence of features in the electronic density of states $N(E)$ near the Fermi level. One of the interesting reasons for the emergence of such features of $N(E)$ is the presence of nematic fluctuations and associated energy splitting of bands formed by d_{xz}/d_{yz} orbitals of iron, which was shown using ARPES by other groups in Ba-122.

REFERENCES

1. Y. Kamihara, H. Hiramatsu, M. Hirano et al., J. Am. Chem. Soc. **128**, 10012 (2006).
2. J. Paglione and R. L. Greene, Nature Phys. **6**, 645 (2010).
3. J. D. Weiss, C. Tarantini, J. Jiang et al., Nature Mater. **11**, 682 (2012).
4. H. Hosono, A. Yamamoto, H. Hiramatsu, and Y. Ma, Materials Today **21**, 278 (2018).
5. X. Lu, *Phase Diagram and Magnetic Excitations of : A Neutron Scattering Study,* Springer, Singapore (2017).
6. S. Ideta, T. Yoshida, I. Nishi et al., Phys. Rev. Lett. **110**, 107007 (2013).
7. D. V. Evtushinsky, V. B. Zabolotnyy, L. Harnagea et al., Phys. Rev. B. **87**, 094501 (2013).
8. A. A. Kordyuk, V. B. Zabolotnyy, D. V. Evtushinsky et al., J Supercond. Nov. Magn. **26**, 2837 (2013).
9. R. S. Dhaka, S. E. Hahn et al., Phys. Rev. Lett. **110**, 067002 (2013).
10. T. E. Kuzmicheva, S. A. Kuzmichev, K. S. Pervakov, and V. A. Vlasenko, JETP Lett. **118**, 514 (2023).
11. T. E. Kuzmicheva, S. A. Kuzmichev, K. S. Pervakov, and V. A. Vlasenko, Phys. Rev. B **104**, 174512 (2021).
12. A. V. Sadakov, A. V. Muratov, S. A. Kuzmichev et al., JETP Lett. **116**, 708 (2022).
13. Yu. A. Aleshchenko, A. V. Muratov, G. A. Ummarino et al., J. Phys.: Cond. Matter. **33**, 045601 (2021).
14. G. A. Ummarino, A. V. Muratov, L. S. Kadyrov et al., Supercond. Sci. Technol. **33**, 075005 (2020).
15. T. E. Kuzmicheva, A. V. Muratov, S. A. Kuzmichev et al., Physics-Uspekhi **60**, 419 (2017).
16. I. I. Mazin, D. J. Singh, M. D. Johannes, M. H. Du, Phys. Rev. Lett. **101**, 057003 (2008).
17. H. Kontani and S. Onari, Phys. Rev. Lett. **104**, 157001 (2010).
18. M. Yi, D. Lu, J.-H. Chu et al., PNAS **108**, 6878 (2011).
19. T. Shimojima, T. Sonobe, W. Malaeb et al., Phys. Rev. B **89**, 045101 (2014).
20. T. Sonobe, T. Shimojima, A. Nakamura et al., Sci. Rep. **8**, 2169 (2018).
21. P. Szabó, Z. Pribulová, G. Pristás, S. L. Bud'ko, P. C. Canfield, P. Samuely, Phys. Rev. B **79**, 012503 (2009).
22. S. Onari and H. Kontani, Phys. Rev. Research **2**, 042005(R) (2020).
23. T. Timusk, B. Statt, Rep. Prog. Phys. **62**, 61 (1999).
24. S. Hüfner, M. A. Hossain, A. Damascelli, G. A. Sawatzky, Rep. Progr. Phys. **71**, 062501 (2008).
25. M. V. Sadovskii, Physics-Uspekhi **44**, 515 (2001).
26. S. Onari and H. Kontani, Phys. Rev. B **100**, 020507(R) (2019).
27. A. E. Karakozov, M. V. Magnitskaya, L. S. Kadyrov, and B. P. Gorshunov, Phys. Rev. B **99**, 054504 (2019).
28. I. A. Nikitchenkov, A. D. Ilina, V. M. Mikhailov et al., Moscow Univ. Phys. Bull **78**, 521 (2023).
29. K. S. Pervakov, V. A. Vlasenko, E. P. Khlybov et al., Supercond. Sci. Technol. **26**, 015008 (2013).
30. Yu. F. Eltsev, K. S. Pervakov, V. A. Vlasenko et al., Physics-Uspekhi **57**, 827 (2014).
31. V. A. Vlasenko, O. A. Sobolevskiy, A. V. Sadakov et al., JETP Letters. **107**, 121 (2018).
32. J. Moreland and J. W. Ekin, J. Appl. Phys. **58**, 3888 (1985).
33. S. A. Kuzmichev and T. E. Kuzmicheva, Low. Temp. Phys. **42**, 1008 (2016).
34. M. Octavio, M. Tinkham, G. E. Blonder, and T. M. Klapwijk, Phys. Rev. B **27**, 6739 (1983).
35. D. Averin and A. Bardas, Phys. Rev. Lett. **75**, 1831 (1995).
36. F. Massee, S. de Jong, Y. Huang et al., Phys. Rev. B **80**, 140507(R) (2009).
37. R. Kümmel, U. Gunsenheimer, and R. Nicolsky, Phys. Rev. B **42**, 3992 (1990).
38. Z. Popović, S. Kuzmichev, and T. Kuzmicheva, J. Appl. Phys. **128**, 013901 (2020).
39. T. E. Kuzmicheva, S. A. Kuzmichev, and N. D. Zhigadlo, Phys. Rev. B **100**, 144504 (2019).
40. Yu. V. Sharvin, Sov. Phys. JETP **21**, 655 (1965).
41. G. Wexler, Proc. Phys. Soc. **89**, 927 (1966).
42. Yu. G. Naidyuk and I. K. Yanson, *Point-Contact Spectroscopy*, Springer, New York (2005).
43. I. Giaever and K. Megerle, Phys. Rev. **112**, 1101 (1961).
44. F. Massee, Y. K. Huang, J. Kaas et al., EPL **92**, 57012 (2010).